AJS American Journal of Science
publishing earth-sciences research since 1818

Zhao, M., Beaty, B., Tarhan, L., & Planavsky, N. (2023). Resetting of Shallow-Water Carbonate Boron Isotope Values During Marine Burial Diagenesis. *American Journal of Science*, *323*, 11. https://doi.org/10.2475/001c.91398

Science Paper

Resetting of Shallow-Water Carbonate Boron Isotope Values During Marine Burial Diagenesis

Mingyu Zhao[1,2][a], Brian Beaty[2], Lidya Tarhan[2], Noah Planavsky[2]

[1] Key Laboratory of Cenozoic Geology and Environment, Institute of Geology and Geophysics, Chinese Academy of Sciences, [2] Department of Earth and Planetary Sciences, Yale University

Keywords: carbonate, marine burial diagenesis, proxy, boron isotopes, recrystallization

https://doi.org/10.2475/001c.91398

American Journal of Science

Vol. 323, 2023

The boron isotopic composition ($\delta^{11}B$) of bulk carbonates may provide an archive to reconstruct changes in ocean pH. Reconstructions from ancient carbonates typically assume that no significant resetting of $\delta^{11}B$ occurred during marine burial diagenesis. However, our understanding of B isotopic behavior associated with this process remains limited. Here we provide measurements of B/Ca and B isotopic composition ($\delta^{11}B$) from a modern peri-platform carbonate sequence near the Great Bahama Bank that has undergone marine burial diagenesis. Our results reveal significant decreases in both $\delta^{11}B$ (~13 ‰) and B/Ca (~80 %) of bulk carbonates with depth. We attribute this pattern to the release of isotopically light B ($\delta^{11}B$ ~20 ‰) to porewater during aragonite dissolution, with uptake of substantially isotopically lighter borate ions ($\delta^{11}B$ ~-1 ‰) from porewater by newly forming low-Mg calcite. A quantitative model adds further support for this interpretation and provides an estimate of average neomorphism rate (k_0) in the range of 1×10^{-6} to 5×10^{-6} yr^{-1}, which is comparable to previous rate estimates for neomorphism and/or recrystallization during meteoric diagenesis. Our results demonstrate the strong potential for resetting $\delta^{11}B$ signatures in bulk carbonates during recrystallization, which must be considered in future attempts to reconstruct pH and pCO_2 from these records and may require reinterpretation of existing records. Our results also suggest the potential of B isotopes as a proxy for carbonate recrystallization/neomorphism and original carbonate mineralogy.

1. INTRODUCTION

The boron isotope values ($\delta^{11}B$) of bulk carbonate sediments have been used to track changes in marine pH and atmospheric pCO_2 during critical events in Earth's history such as the termination of Snowball Earth and the Permian-Triassic mass extinction (Clarkson et al., 2015; Kasemann et al., 2005, 2010; Ohnemueller et al., 2014). Carbonate $\delta^{11}B$ values may also be able to provide insights into microenvironments under which carbonates precipitated. For instance, calcifying algae have anomalously positive $\delta^{11}B$ values (Donald et al., 2017; Zhang et al., 2017). Using carbonate $\delta^{11}B$ values as environmental proxies in ancient carbonates rests on the assumption that no significant B isotopic resetting during diagenesis—which may occur when carbonates undergo recrystallization (no change in mineral phases) or neomorphism (transformation of metastable high-Mg calcite or aragonite to low-Mg calcite or dolomite) (Knauth & Kennedy, 2009; Land, 1986). Carbonate diagenesis can be broadly subdivided into meteoric and mixing zone diagenesis, marine burial diagenesis, and deep burial diagenesis based on the composition of the diagenetic fluid and the depth of burial (e.g., Marshall, 1992; Oehlert & Swart, 2014; M. Y. Zhao, Planavsky, et al., 2020; M. Y. Zhao & Zheng, 2017). Platform carbonates altered by meteoric diagenesis on the Great Bahama Bank record significant reductions in both $\delta^{11}B$ and B/Ca values (Stewart et al., 2015) but the influence of marine burial diagenesis on shallow-water carbonate $\delta^{11}B$ beyond the zone of meteoric alteration remains underexplored.

The basis for boron as a pH proxy is that the relative distribution of the two aqueous boron species, boric acid $B(OH)_3$ and the borate ion $B(OH)_4^-$, is a function of pH and there is a large isotopic fractionation between these two species. The boron isotopic fractionation between $B(OH)_3$ and $B(OH)_4^-$ is ~26 ‰ at 25 °C in seawater, with light ^{10}B preferentially incorporated into $B(OH)_4^-$ (Klochko et al., 2006; Nir et al., 2015). Borate ions are, in turn, preferentially incorporated into carbonate crystal lattices. Therefore, the B isotopic fractionation between carbonate and seawater is a function of pH. Consequently, the B isotopic composition of carbonates can be used to calculate the pH

a Corresponding author: mingyu.zhao@mail.iggcas.ac.cn

of seawater as long as the B isotopic composition of seawater is known.

Marine burial diagenesis in carbonate platforms is usually characterized by the transformation of metastable carbonates such as aragonite and high-Mg calcite to stable low-Mg calcite and dolomite (e.g., Malone et al., 2001; Melim et al., 2002; M. Y. Zhao, Planavsky, et al., 2020). On the other hand, the main pathway for marine burial diagenesis in deep-sea carbonates is the recrystallization of calcite with varying Mg contents (e.g., Brown & Elderfield, 1996; Fantle et al., 2010; Swart & Eberli, 2005). Regardless of the setting, the interaction between primary carbonate and marine porewater may significantly alter carbonate composition (e.g., Fantle et al., 2010; Higgins et al., 2018), even if the composition of marine porewater is similar to that of seawater. Many studies indicate that marine burial diagenesis significantly impacts both elemental (e.g., Mg/Ca and Sr/Ca) and isotopic records (e.g., $\delta^{13}C$, $\delta^{18}O$, $\delta^{44}Ca$, $\delta^{238}U$, and $\delta^{7}Li$) of marine carbonates (e.g., Brown & Elderfield, 1996; Chen et al., 2018; Dellinger et al., 2020; Fantle et al., 2010; Higgins et al., 2018; Swart & Eberli, 2005; M. Y. Zhao & Zheng, 2014), although a recent study suggests that it does not have a big impact on the Ce anomaly of carbonates (Liu et al., 2019). In contrast, the effects of marine burial diagenesis on the B isotope signatures of shallow-water carbonates remain comparatively understudied.

A few studies have investigated B isotopic variation in deep-sea carbonates during marine burial diagenesis (Edgar et al., 2015; Spivack et al., 1993; Spivack & You, 1997). These studies have revealed that the extent of alteration of $\delta^{11}B$ in deep-sea carbonates is site-specific, which could be related to the original mineral composition and/or porewater conditions. For example, the recrystallization of bulk carbonates at ODP Site 851 corresponds with a drop in $\delta^{11}B$ (Spivack & You, 1997). However, these changes were not observed in other deep-sea sites characterized chiefly by foraminiferal calcite (ODP Sites 803 and 865, TDP Site 18, Edgar et al., 2015; Spivack et al., 1993). While these studies are useful for interpreting $\delta^{11}B$ in deep-sea marine sedimentary archives, these sites are likely poor analogues for marine carbonate platforms. Application of the $\delta^{11}B$ pH and pCO_2 proxy to ancient rock records, therefore, will benefit from a better understanding of B isotope behavior in modern carbonate platforms during marine burial diagenesis.

Here we provide $\delta^{11}B$ and B/Ca measurements from an extensively studied carbonate core (ODP Leg 166 Site 1007) collected near the Great Bahama Bank to understand the influence of marine burial diagenesis on the B/Ca and $\delta^{11}B$ values of platform bulk carbonate sediments.

2. MATERIALS AND METHODS

2.1. Study site and samples

The studied ODP Leg 166 Site 1007 (24°30.261′N, 79°19.34′W, fig. 1) has a total cored depth of 1250 m, which consists mainly of carbonates deposited from the early Miocene to present. The current water depth of this site is around 700 m (fig. 1, Shipboard Scientific Party, 1997). This site is rich in foraminifera fossils, and an age model based on nannofossil zonation shows that it was formed during the last 20 Myrs, with sedimentation rates in the range of 0.001 to 0.021 cm yr^{-1} (Shipboard Scientific Party, 1997). Due to its much greater water depth than the nearby Clino and Unda cores (Swart & Eberli, 2005), meteoric diagenesis has not impacted this site. This is also supported by the $\delta^{18}O_{carb}$ values (~0 ‰), which do not show negative shifts typical of meteoric diagenesis (e.g., Frank & Bernet, 2000; Stewart et al., 2015). The Site 1007 core thus provides an opportunity to study the effects of marine burial diagenesis on platformal carbonates. The studied sequence can be divided into two mineralogically distinct intervals (fig. 2A). The upper interval (0–203 meters below seafloor [mbsf]) is mainly made up of aragonite (~65 %) and low-Mg calcite (~25 %), with minor contributions from high-Mg calcite (<5 %) (Shipboard Scientific Party, 1997). The lower interval (203–1100 mbsf) is mainly made up of low-Mg calcite (~80 %), with small amounts of aragonite (0–20 %) and dolomite (0–20 %) (Shipboard Scientific Party, 1997).

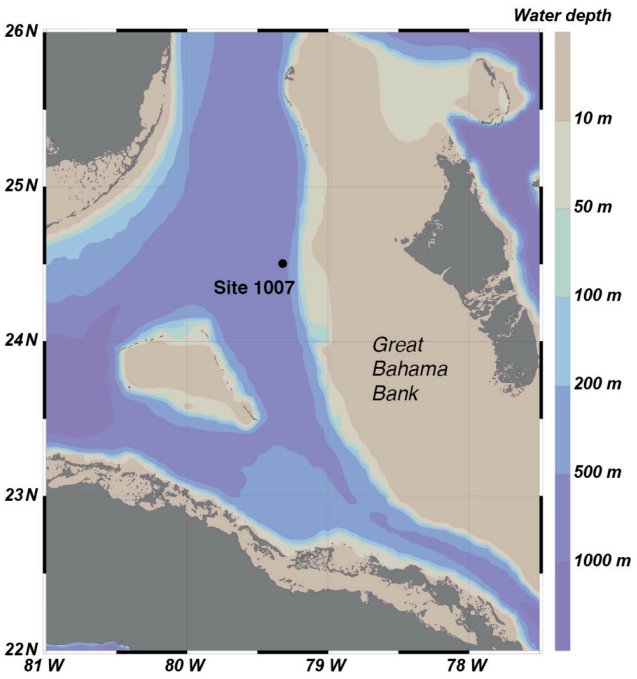

Figure 1. Map of the study site offshore of the Great Bahama Bank.

Color gradient denotes water depth. Figure generated using Ocean Data View. Schlitzer, R., (2018), Ocean Data View, https://odv.awi.de.

Site 1007 as well as nearby sites (such as ODP Site 1006) have been extensively studied to understand the influence of marine burial diagenesis on various isotopic systems such as C isotopes (Swart & Eberli, 2005), Li isotopes (Dellinger et al., 2020), U isotopes (Chen et al., 2018), and Ca and Mg isotopes (Higgins et al., 2018). Thus, these sites provide a unique window to pinpoint the effect of marine burial diagenesis on the B isotopic system in platform carbonate sediments, which can be regarded as an ideal ana-

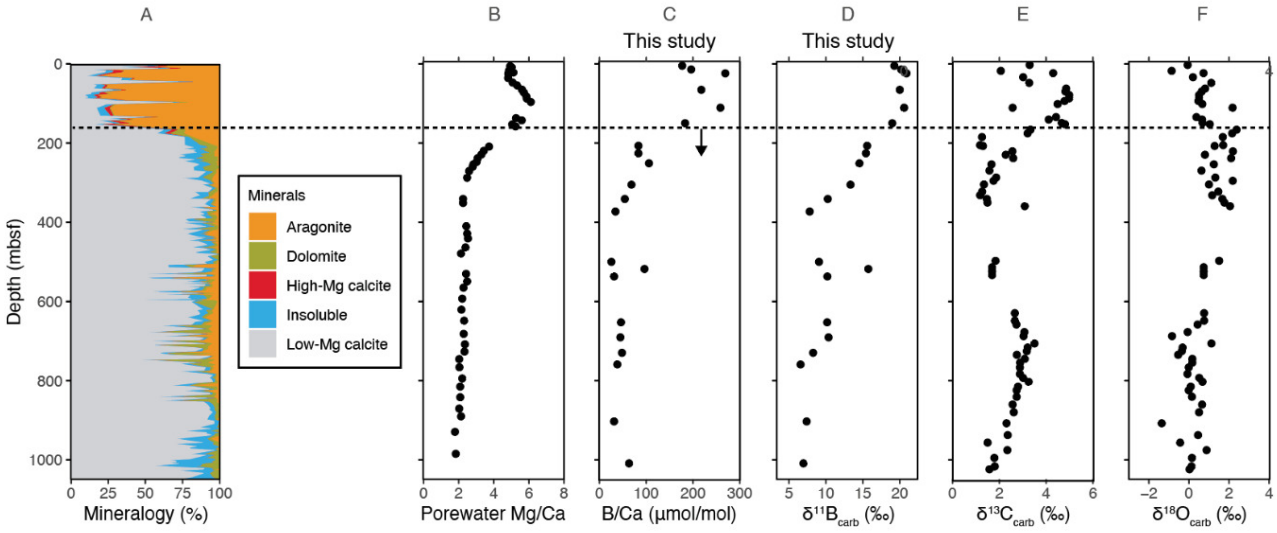

Figure 2. Sedimentary geochemical results from ODP Site 1007.

A. Mineralogical composition. B. Mg/Ca molar ratio of porewater. C. B/Ca value of bulk carbonate sediments (i.e., the composite signature of all carbonates in these samples). D. $\delta^{11}B$ value of bulk carbonate sediments. E. $\delta^{13}C$ value of bulk carbonate sediments. F. $\delta^{18}O$ of bulk carbonate sediments. Mineralogical (A) and porewater Mg/Ca (B) data from Shipboard Scientific Party (1997). Sedimentary $\delta^{13}C_{carb}$ (E) and $\delta^{18}O_{carb}$ (F) data from Higgins et al. (2018). The horizontal dashed line denotes the stratigraphic level below which neomorphism notably increases. The analytical errors for B/Ca and $\delta^{11}B$ are smaller than the size of the symbols.

logue for a wide range of commonly analyzed ancient carbonate rocks.

2.2. Sample digestion

A total of 21 samples from the studied site were analyzed for B/Ca and $\delta^{11}B$ values (fig. 2) following the method described in Foster (2008), Zhang et al. (2017) and Henehan et al. (2019). About 10 mg of powdered bulk samples were weighed for digestion. The carbonate digestion follows the procedures described by Zhang et al. (2017) and Henehan et al. (2019). First, the samples were ultrasonicated and rinsed with MQ water five times to remove clays. Further, an oxidizing mixture (1 % H_2O_2 with 0.1 M NH_4OH) was used to oxidize organic matter present in the samples. In this step, the samples and the oxidizing mixture were heated to 80 ^oC in a water bath for 15 min, with 15 s ultrasonication every 5 min. Thereafter, 250 µL of 0.0005 M HNO_3 were added to the samples to remove re-adsorbed contaminants. Following this, excess 0.5 M HNO_3 (<500 µL) were added for 5 minutes to dissolve carbonates and leave behind insoluble clays, if present. Finally, the dissolved samples were centrifuged for 2–5 minutes, and the supernatant was transferred to clean Teflon vials. No residue was observed in the centrifuged samples before the supernatant was extracted.

2.3. B/Ca measurement

A split of the supernatant (20 µL) was used for B/Ca measurement via a Thermo Element XR ICP-MS at the Yale Metal Geochemistry Center (YMGC). A B-clean Teflon barrel spray chamber, torch, and cones were used to reduce background B content. Several in-house standards were used to monitor the uncertainty of the measurement. B/Ca and Ca concentrations of the bracketing standards were also adjusted to match those of the samples. The external precision (2σ) is better than 5 %, as revealed through repeated analysis of the in-house standards and sample duplicates.

2.4. Sample purification

The B purification was done using Teflon columns with 20 µL of 63–100 µm boron-specific anionic exchange resin Amberlite IRA 743 following a well-established protocol (Foster, 2008; Henehan et al., 2019; Zhang et al., 2017). Before the column procedures, B-free acetic acid-Na acetate buffer was added to samples to ensure pH>5. The columns were first cleaned using 2.5 mL of 0.5 M HNO_3 and then pre-conditioned using 2 mL of MQ water. The buffered samples were loaded slowly into the columns using pipettes to avoid either the suspension of the resin or the formation of small sample drops on the inner walls of the column reservoirs. Further, 10 aliquots of 160 µL of MQ water were added to remove the matrix from the resin and the inner walls of the columns. Boron was then eluted through the addition of 5 aliquots of 120 µL 0.5 M HNO_3. The elution tails were further collected using an additional 120 µL 0.5 M HNO_3 to check for incomplete B recovery in sample vials. A total procedural blank and a JCp-1 carbonate standard were added to each batch to monitor potential contamination as well the accuracy of the measurement. All newly constructed columns were tested for potential column fractionation before use by running B-purified NIST SRM boric acid standard 951 and ensuring that each measurement fell within 0.00 ± 0.10 ‰.

2.5. $\delta^{11}B$ measurement

Boron isotopic compositions were measured on a Thermo Neptune Plus MC-ICP-MS at the Yale Metal Geochemistry Center (YMGC), following the procedure described in Foster (2008), Zhang et al. (2017), and Henehan et al. (2019). A separate B-clean Teflon barrel spray chamber was used to avoid contamination during measurement. Ammonia gas was added to improve B washout. Samples were bracketed by NIST SRM 951 boric acid reference standards. Boron isotopic results were reported in δ-notation ($\delta^{11}B$) relative to NIST SRM 951. The total procedural blanks were in the range of 0 to 59.9 pg of B, which is much smaller than the size of the samples (>10 ng B). Thus, the influence of total procedural blanks on the $\delta^{11}B$ results of samples is minor (<0.2 ‰). The $\delta^{11}B$ of the JCp-1 standard was 24.26 ± 0.19 ‰ (2σ, n=4), consistent with reported values (Gutjahr et al., 2021; McCulloch et al., 2014; Zhang et al., 2017). This also suggests an external precision of ~0.2 ‰ (2σ) for these measurements. Two more boric acid standards, AE120 and AE121, were measured to monitor the precision and accuracy of sample measurements (Vogl & Rosner, 2012). The measured values for AE120 and AE121 were -20.33 ± 0.17 ‰ (2σ, n=11) and 19.56 ± 0.15 ‰ (2σ, n=11), respectively. These results compare well with values previously reported by Zhang et al. (2017) (-20.27 ± 0.23 ‰ and 19.54 ± 0.15 ‰, respectively) and Stewart et al. (2021) (19.71 ± 0.07 ‰ for AE121).

2.6. Diagenetic modeling

To simulate the changes we observed in the B/Ca and $\delta^{11}B$ values of carbonates in the studied ODP Leg 166 Site 1007, we built a simple diagenetic model that includes five components: the amount of aragonite in sediments, [B] and [^{10}B] of porewater, and [B] and [^{10}B] of carbonates (aragonite and diagenetically formed calcite). The only reaction in the model is the neomorphism of aragonite to low-Mg calcite. Dissolution and reprecipitation processes without a net change in the amount of carbonate were used to simulate this neomorphism process. The mass balance equation for aragonite in sediments (A) is (cf. Berner, 1980):

$$\frac{\partial A}{\partial t} = -\frac{\partial}{\partial z}(\omega A) - kA \quad (1)$$

where ω is the advection rate of sediments, k is the rate of neomorphism of aragonite to low-Mg calcite, and z is depth (positive downward). The mass balance equations for the other components are (following Berner, 1980; Tarhan et al., 2021; M. Zhao et al., 2023; M. Y. Zhao et al., 2021; M. Y. Zhao, Planavsky, et al., 2020; M. Y. Zhao, Zhang, et al., 2020):

$$\frac{\partial C_l}{\partial t} = \frac{\partial}{\partial z}\left(D\frac{\partial C_l}{\partial z}\right) - \frac{\partial}{\partial z}(vC_l) + k\frac{1-\phi}{\phi}A(R_i - R_{eq}) \quad (2)$$

$$\frac{\partial C_s}{\partial t} = -\frac{\partial}{\partial z}(\omega C_s) - kA(R_i - R_{eq}) \quad (3)$$

where C_l represents [^{10}B] or [B] in porewater, C_s represents [^{10}B] or [B] in carbonates, D is the coefficient of molecular diffusion, v is the advection rate of pore water, ϕ is porosity, and R_i is the initial [^{10}B]/[Ca] or [B]/[Ca] ratio in aragonite. R_{eq} represents the [^{10}B]/[Ca] or [B]/[Ca] ratio in carbonates that is in equilibrium with porewater. The effect of tortuosity on diffusion is included as $D = \frac{D_m}{1-2\ln(\phi)}$, where D_m is the intensity of molecular diffusion in seawater. The original geochemical composition of the carbonates (B/Ca and $\delta^{11}B_{carb}$) was set to be the same as that observed in the upper sediments at Site 1007 (<160 m). The effect of compaction on the advection rates of carbonates and porewater was included in the calculation, following Berner (1980). The porosity in the model was set as a function of depth by fitting the real data shown in Shipboard Scientific Party (1997). The fitting equation is $\phi(z) = \phi_\infty + (\phi_0 - \phi_\infty)\exp(-z/\lambda)$, where ϕ_0 and ϕ_∞ represent porosity at the top of the sediment column and at depth, respectively, and λ is the porosity attenuation length. Model components and boundary conditions are shown in table 1. Model parameters can be found in table 2. The main equations for each component in the model are shown in table 3. The pH of porewater is fixed at 7.5, following data reported by Shipboard Scientific Party (1997). The R_{eq} of [B]/[Ca] in carbonates was set as a function of porewater [B] ($[B]_p$):

$$R_{eq} = KD_b * [B]_p \quad (4)$$

where KD_b is the partition coefficient of [B]/[Ca] between low-Mg calcite and porewater. The R_{eq} for [^{10}B]/[Ca] of carbonates was calculated under the assumption that the B of newly formed calcite is mainly from $B(OH)_4^-$ of the porewater (pH = 7.5; Shipboard Scientific Party, 1997) at the study site (Noireaux et al., 2015):

$$\left(\frac{[^{11}B]}{[^{10}B]}\right)_{cal} = \left(\frac{[^{11}B]}{[^{10}B]}\right)_{borate} \quad (5)$$

where $\left(\frac{[^{11}B]}{[^{10}B]}\right)_{cal}$ is the $^{11}B/^{10}B$ ratio of newly formed calcite and $\left(\frac{[^{11}B]}{[^{10}B]}\right)_{borate}$ is the $^{11}B/^{10}B$ ratio of borate in porewater. Thus, a series of equations is required to calculate the ^{10}[B]/[B] ratio of newly formed calcite ($\left(\frac{[^{10}B]}{[B]}\right)_{cal}$) in the main equation of carbonate [^{10}B] from [^{10}B] and [B] of porewater (table 3). First, the $^{11}B/^{10}B$ ratio of porewater ($\left(\frac{[^{11}B]}{[^{10}B]}\right)_{pw}$) can be calculated from [^{10}B] and [B] of porewater ($[^{10}B]_{pw}$ and $[B]_{pw}$) using:

$$\left(\frac{[^{11}B]}{[^{10}B]}\right)_{pw} = \frac{[B]_{pw} - [^{10}B]_{pw}}{[^{10}B]_{pw}} \quad (6)$$

The fraction of borate (f_{borate}) in porewater is a function of pH:

$$f_{borate} = \frac{K_B}{K_B + [H]} \quad (7)$$

where K_B is the dissociation constant of boric acid. Further, the $^{11}B/^{10}B$ ratio of borate can be calculated from $\left(\frac{[^{11}B]}{[^{10}B]}\right)_{pw}$ and f_{borate} using:

$$\left(\frac{[^{11}B]}{[^{10}B]}\right)_{borate} = \frac{\left(\frac{[^{11}B]}{[^{10}B]}\right)_{pw}}{f_{borate} + (1 - f_{borate})\alpha} \quad (8)$$

where α is the B isotopic fractionation between boric acid and borate, which is set as 26 ‰ following the study of Nir et al. (2015). $\left(\frac{[^{11}B]}{[^{10}B]}\right)_{cal}$ can then be calculated using equations (5) and (8). Finally, $^{10}B/B$ of newly formed calcite can be calculated from $\left(\frac{[^{11}B]}{[^{10}B]}\right)_{cal}$, using:

Table 1. Chemical species and boundary conditions for the diagenetic model

	Species	Boundary condition	Unit
Solid	Aragonite (A)	J.A = $\omega_0 * \frac{1000\rho}{100} * (1\text{-}\phi_0) * f_{iarag}$	mmol cm^{-2} yr^{-1}
	Carbonate [B] (B_{carb})	$(B/Ca)_i$ =315×10^{-6} for aragonite	mol/mol
	Carbonate [^{10}B] ($^{10}B_{carb}$)	$\delta^{11}B_i$ = 20	‰
Solute	Porewater [B] (B_{pw})	B_{pwi} = 416×10^{-6}	mol L^{-1}
	Porewater [^{10}B] ($^{10}B_{pw}$)	$\delta^{11}B_{pwi}$ = 39.61	‰

$$\left(\frac{[^{10}B]}{[B]}\right)_{cal} = \frac{1}{1+\left(\frac{[^{11}B]}{[^{10}B]}\right)_{cal}} \quad (9)$$

Following findings that the recrystallization rate of deep-sea carbonates decreases exponentially with depth (Fantle & DePaolo, 2007), the rate of neomorphism (k) is also set as an exponential attenuation function of depth. The attenuation of k with depth is consistent with the fact that aragonite is not fully transformed into low-Mg calcite even at depth (>800 m, fig. 2). The rate was set as zero for the upper 140 m, since the relatively high concentration of aragonite in these sediments does not support neomorphism above this depth. Thus, the expression of the rate constant is:

$$k = \begin{cases} 0, & z < 140\ m \\ k_0 e^{-\frac{z-140}{\lambda_k}}, & z > 140\ m \end{cases} \quad (10)$$

where k_0 and λ_k are the rate constant of neomorphism and the attenuation length, respectively. The parameters k_0 and λ_k were estimated by fitting aragonite percentage as well as B/Ca and δ^{11}B data of carbonates. Note that the above neomorphism model only describes aragonite and the low-Mg calcite formed through neomorphism. It does not include initial low-Mg calcite in the sediments, which at Site 1007 accounts for ~25 % of carbonate sediments in the upper intervals of the core. Thus, the results of the model were calibrated to consider the proportion of initial carbonate sediments comprised of low-Mg calcite through:

$$\left(\frac{B}{Ca}\right)_{fcarb} = \left(\frac{B}{Ca}\right)_{mcarb} * f_{iarag} + \left(\frac{B}{Ca}\right)_{ical} * (1 - f_{iarag}) \quad (11)$$

where $\left(\frac{B}{Ca}\right)_{fcarb}$ is the final model-generated carbonate B/Ca value after calibration of initial calcite, $\left(\frac{B}{Ca}\right)_{mcarb}$ is the carbonate B/Ca value determined from the above neomorphism model, f_{iarag} is the initial portion of aragonite in the sediments, and $\left(\frac{B}{Ca}\right)_{ical}$ is the B/Ca value of the initial calcite in sediments, which was set to be the same as the B/Ca value of the final carbonates (bulk carbonate sediments) at depth (45×10^{-6} mol/mol). Similar to equation (11), the final model-generated carbonate δ^{11}B after calibration of initial calcite ($\delta^{11}B_{fcarb}$) is calculated using:

$$\delta^{11}B_{fcarb} = \frac{\delta^{11}B_{mcarb} * \left(\frac{B}{Ca}\right)_{mcarb} * f_{iarag} + \delta^{11}B_{ical} * \left(\frac{B}{Ca}\right)_{ical} * (1 - f_{iarag})}{\left(\frac{B}{Ca}\right)_{fcarb}} \quad (12)$$

where $\delta^{11}B_{mcarb}$ is the carbonate δ^{11}B resulting from the above neomorphism model, and $\delta^{11}B_{ical}$ is the δ^{11}B of initial calcite in sediments.

The model was written in R. The thickness of the sediment pile was set as 1000 m, which was divided into 100 layers of uniform (10 m) thickness. The model was solved numerically using the Method of Lines through the Variable Coefficient Ordinary Differential Equations (VODE) solver (Soetaert et al., 2010). The model was run to steady state to calculate the depth distribution of the geochemical compositions of both pore water and carbonates.

3. RESULTS

As shown in fig. 2 and table 4, our analyses indicate that both B/Ca and $\delta^{11}B_{carb}$ values of Site 1007 sediments decrease with depth. B/Ca is approximately 220 µmol/mol for the upper 160 m, followed by a decrease from ~220 to ~50 µmol/mol between 160 and 400 mbsf. Finally, B/Ca stabilizes at ~50 µmol/mol below 400 mbsf. Variation in $\delta^{11}B_{carb}$ appears to extend deeper than that of B/Ca. The $\delta^{11}B_{carb}$ value is approximately 20 ‰ in the upper 160 m, with a gradual decrease from 20 ‰ to ~7.0 ‰ between 160 and 750 mbsf. Below 750 mbsf, $\delta^{11}B_{carb}$ is relatively stable around 7 ‰.

Significant changes in B/Ca and $\delta^{11}B_{carb}$ occur around 160–250 mbsf. Previous measurements from the core reveal a dramatic change in mineral composition at the same depth (fig. 2; Shipboard Scientific Party, 1997). The percentage of aragonite decreases from ~70 % to ~10 %, whereas the percentage of calcite increases from ~20 % to 80 % (fig. 2). The amount of dolomite also increases below this level, which corresponds closely with a decrease in porewater Mg/Ca (fig. 2; Shipboard Scientific Party, 1997). Moreover, across the same depth range, there is also a considerable decrease in the δ^{13}C value of carbonate from ~4 ‰ to ~ 2 ‰ (fig. 2; Higgins et al., 2018; Swart & Eberli, 2005).

4. DISCUSSION AND DIAGENETIC MODELING

4.1. Evaluation of clay contamination on $\delta^{11}B_{carb}$

Clay contamination may alter the δ^{11}B values of bulk carbonates, but we consider the effect to be negligible in our samples, as discussed below. The effect of clay contamination on $\delta^{11}B_{carb}$ has been explored experimentally, using mixtures of clays and carbonates (Deyhle & Kopf, 2004). The results show that, in a worst-case scenario, six hours of

Table 2. The parameters of the diagenetic model

Symbol	Description	Value	Unit	Sources
ϕ_0	Initial porosity	0.5	1	SSP (1997)
ϕ_∞	Porosity at depth	0.25	1	SSP (1997)
λ	Attenuation coefficient for porosity profile	100	m	SSP (1997)
ρ	Density of sediments	2.0	g cm^{-3}	SSP (1997)
ω_0	Sedimentation rate	0.005 to 0.02	cm yr^{-1}	SSP (1997)
k_0	Neomorphism rate constant	2×10^{-6}	yr^{-1}	Zhao, Planavsky et al. (2020); this study
λ_k	Attenuation length for the rate of neomorphism	200	m	This study
f_{iarag}	Portion of aragonite in the initial carbonates	0.65	1	This study
$(B/Ca)_{ical}$	B/Ca of initial calcite	45×10^{-6}	mol/mol	This study
$\delta^{11}B_{ical}$	B/Ca of initial calcite	20	‰	Zhang et al. (2017); this study
K_B	Dissociation constant of boric acid	1.708×10^{-9}	mol L^{-1}	Dickson (1990)
D_m	Molecular diffusion of B in porewater	230	cm^2 yr^{-1}	Boudreau (1997)
KD_b	Partition coefficient of [B]/[Ca] between low-Mg calcite and porewater	0.006	mol^{-1} g	Allen & Hönisch (2012)
α	B isotopic fractionation between boric acid and borate ion	26	‰	Nir et al. (2015)

Note: SSP (1997) represents Shipboard Scientific Party (1997).

Table 3. Main equations for the model components

Species	Equations
A	$\frac{\partial A}{\partial t} = -\frac{\partial}{\partial x}(\omega A) - kA$
B_{carb}	$\frac{\partial (B_{carb})}{\partial t} = -\frac{\partial}{\partial x}(\omega B_{carb}) - kA((B/Ca)_i - KD_b * [B]_p)$
$^{10}B_{carb}$	$(\frac{[^{11}B]}{[^{10}B]})_{pw} = \frac{[B]_{pw}-[^{10}B]_{pw}}{[^{10}B]_{pw}}$ $f_{borate} = \frac{K_B}{K_B+[H]}$ $(\frac{[^{11}B]}{[^{10}B]})_{borate} = \frac{(\frac{[^{11}B]}{[^{10}B]})_{pw}}{f_{borate}+(1-f_{borate})\alpha}$ $(\frac{[^{11}B]}{[^{10}B]})_{cal} = (\frac{[^{11}B]}{[^{10}B]})_{borate}$ $(\frac{[^{10}B]}{[B]})_{cal} = \frac{1}{1+(\frac{[^{11}B]}{[^{10}B]})_{cal}}$ $\frac{\partial (^{10}B_{carb})}{\partial t} = -\frac{\partial}{\partial x}(\omega^{10}B_{carb}) - kA(\left(\frac{^{10}B}{Ca}\right)_i - KD_b * [B]_p * (\frac{[^{10}B]}{[B]})_{cal})$
B_{pw}	$\frac{\partial (B_{pw})}{\partial t} = \frac{\partial}{\partial x}\left(D\frac{\partial B_{pw}}{\partial x}\right) - \frac{\partial}{\partial x}(vB_{pw}) + k\frac{1-\phi}{\phi}A((B/Ca)_i - KD_b * [B]_p)$
$^{10}B_{pw}$	$\frac{\partial (^{11}B_{pw})}{\partial t} = \frac{\partial}{\partial x}\left(D\frac{\partial (^{11}B_{pw})}{\partial x}\right) - \frac{\partial}{\partial x}(v(^{11}B_{pw})) + k\frac{1-\phi}{\phi}A(\left(\frac{^{10}B}{Ca}\right)_i - KD_b * [B]_p * (\frac{[^{10}B]}{[B]})_{cal})$

digestion using 2M HCl induced only a 0.14 ppm increase in B content and a 3 ‰ shift in $\delta^{11}B_{carb}$ in carbonate-dominated mixtures containing 20 % clays. We digested the samples using 0.5 M HNO_3 for five minutes. The B contents of our carbonate samples are higher than 3 ppm (table 5), but the clay contents of our samples are lower than 10 %. Thus, the contamination from structurally-bound B in clays during our digestion procedures should be minor. Moreover, B concentration decreases rather than increases with our measured Al content (table 5), which also cannot be explained by clay contamination.

We have additionally evaluated the contribution of desorbable B (B_{desorb}) from clays in our measurements (table 5). A typical B_{desorb}/Al of 1/9000 for clay was used in this calculation (Paris et al., 2010). The results show that the contribution of B_{desorb} to our $\delta^{11}B_{carb}$ measurements is <1 %. This can generate a maximum $\delta^{11}B_{carb}$ shift of only -0.08 ‰, even if the assumed $\delta^{11}B$ of desorbable B is extremely low (-10 ‰).

Table 4. Geochemical results from ODP Site 1007

Samples	Depth	B/Ca	$\delta^{11}B$	2σ
	mbsf	μmol/mol	‰	‰
1H 02 039-040	4.75	176.7	19.27	0.05
2H 06 039-040	14.25	196.0	20.18	0.06
3H 04 039-040	23.9	269.0	20.90	0.09
7H 06 039-040	65.4	217.9	20.00	0.11
13X CC 040-041	111	258.7	20.58	0.12
17X 04 039-040	150	183.1	18.98	0.05
23X 06 039-040	207	83.4	15.59	0.09
25X 04 039-040	226	83.5	15.43	0.11
28X 02 039-040	251	105.8	14.53	0.10
34X 01 062-063	304.9	68.9	13.31	0.11
38X 01 013-014	341.2	54.3	10.26	0.11
41X CC 027-028	373	34.5	7.81	0.11
21R 03 043-044	500	25.7	9.07	0.12
23R 01 043-044	518	96.3	15.74	0.07
25R 01 045-046	537	31.6	10.20	0.13
37R 08 028-029	653	45.7	10.17	0.16
41R 08 040-041	691	44.8	10.38	0.12
45R 05 040-041	730	48.3	8.25	0.10
48R 05 037-038	759	38.3	6.56	0.13
63R 03 044-045	903	31.5	7.40	0.12
74R 01 040-041	1009	63.4	6.96	0.13

Note: The 2σ here represents internal analytical error based on the standard derivation of the results for 50 analytical cycles of each sample.

4.2. The influence of marine burial diagenesis on $\delta^{11}B_{carb}$

The $\delta^{11}B_{carb}$ values of the top 160 m (~20 ‰) are nearly the same as the pre-industrial $\delta^{11}B$ value of seawater borate ($\delta^{11}B_{borate}$ = 19.7 ‰, Zhang et al., 2017), and they are also comparable to the $\delta^{11}B$ value of core-top ooids from the Bahamas (~22 ‰, Hemming & Hanson, 1992; Zhang et al., 2017). This suggests no significant B isotopic fractionation between aragonite and seawater borate, consistent with previous experimental findings for synthetic aragonite (Henehan et al., 2022; Klochko et al., 2009; Noireaux et al., 2015; Sen et al., 1994).

Unlike the upper 160 m of the core, the decrease in $\delta^{11}B_{carb}$ with depth at Site 1007 is difficult to explain as a primary seawater or depositional signal. Given that reconstructed seawater $\delta^{11}B$ is never more than ~2 ‰ lighter than the modern seawater value (~38–40 ‰) across the 20-Myr depositional duration of the core (fig. 3; cf. Greenop et al., 2017; Rasbury & Hemming, 2017), and estimated changes in atmospheric pCO_2 and marine pH (Beerling & Royer, 2011; Rae et al., 2021) are not large enough to have been the primary drivers of the ~13 ‰ shift we observe, changes in seawater chemistry alone cannot fully explain this decrease in $\delta^{11}B_{carb}$.

An alternative explanation for the observed decrease in $\delta^{11}B_{carb}$ with depth is a change in primary mineral composition and thus B isotopic fractionation between seawater borate and precipitated carbonates. The major mineralogical shift starting from around 160 mbsf at Site 1007 has been explained as reflecting a sediment source change from pelagic low-Mg calcite (i.e., coccoliths and foraminifera) to peri-platform aragonite (derived from calcifying green algae and non-skeletal carbonates) (Swart, 2008; Swart & Eberli, 2005). If a change in mineral composition were the only reason for the observed $\delta^{11}B_{carb}$ shift, it would imply a significant negative fractionation between low-Mg calcite and seawater borate ($\Delta_{carb\text{-}borate}$ = ~-11 ‰). This is, however, much larger than the known fractionation factors between calcite and borate, which are less than 4 ‰ (Henehan et al., 2016; Rae et al., 2011; Rasbury & Hemming, 2017). Thus, a change in primary mineral composition is an unlikely explanation for the observed significant $\delta^{11}B_{carb}$ decrease with depth. Lending some support to our conclusions, a previous study on Ca isotopes at Site 1007 found that changes in primary mineralogy were unlikely to be a driver of Ca isotopic variability (Higgins et al., 2018).

Given our results, a more plausible explanation is that the original mineralogy of the entire core was aragonite and high-Mg calcite, and that marine burial diagenesis resulted in closed-system neomorphism of aragonite to low-Mg calcite at depth. Under this scenario, B release from aragonite to porewater during diagenesis would explain the decrease in carbonate B/Ca values with depth in the core. Given that

Table 5. A calculation of the contribution of desorbable B to our measurements

						Shift in bulk B from clay contamination (‰)	
	Total B (ppm)	Al (ppm)	B/Al (ppm/ ppm)	%B desorb	B_{desorb} (ppb)	$\delta^{11}B_{desorb}$ = -10‰	$\delta^{11}B_{desorb}$ = +20‰
1H	19.4	46.3	0.420	0.026	5.1	0.00	0.00
2H	21.6	50.2	0.429	0.026	5.6	0.00	0.00
3H	29.6	23.3	1.271	0.009	2.6	0.00	0.00
7H	24.0	51.9	0.461	0.024	5.8	0.00	0.00
13X	28.5	27.5	1.037	0.011	3.1	0.00	0.00
17X	20.1	36.4	0.554	0.020	4.0	0.00	0.00
23X	9.2	81.4	0.113	0.099	9.0	-0.01	0.00
25X	9.2	207.4	0.044	0.251	23.0	-0.03	0.01
28X	11.6	77.0	0.151	0.074	8.6	-0.01	0.00
34X	7.6	47.8	0.159	0.070	5.3	-0.01	0.00
38X	6.0	80.9	0.074	0.151	9.0	-0.02	0.01
41X	3.8	103.9	0.036	0.305	11.5	-0.03	0.04
21R	2.8	160.5	0.018	0.632	17.8	-0.06	0.07
23R	10.6	77.2	0.137	0.081	8.6	-0.01	0.00
25R	3.5	170.4	0.020	0.545	18.9	-0.05	0.05
37R	5.0	252.2	0.020	0.557	28.0	-0.06	0.06
41R	4.9	201.0	0.024	0.454	22.3	-0.05	0.04
45R	5.3	392.1	0.014	0.820	43.6	-0.08	0.10
48R	4.2	266.3	0.016	0.703	29.6	-0.07	0.10
63R	3.5	66.9	0.052	0.214	7.4	-0.02	0.03
74R	7.0	456.6	0.015	0.728	50.7	-0.07	0.10

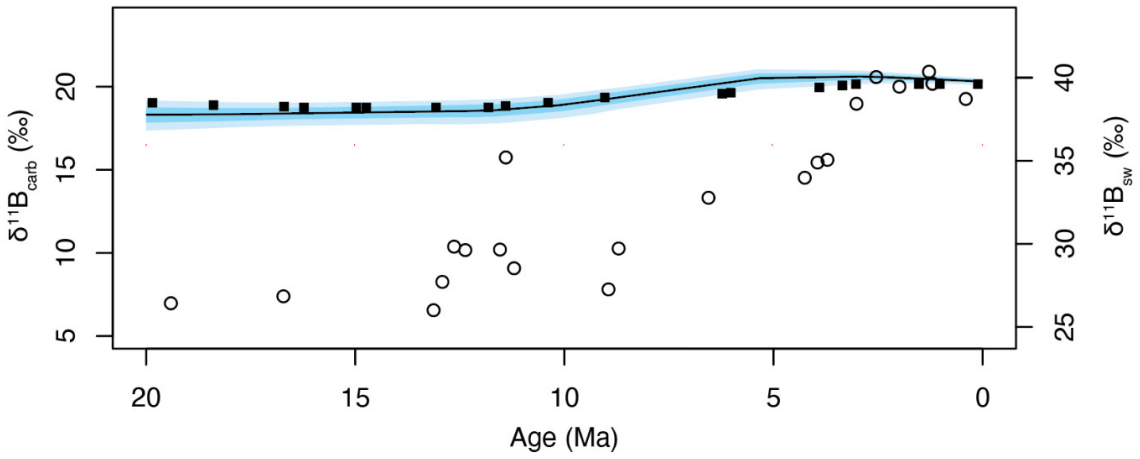

Figure 3. A comparison between $\delta^{11}B$ value of bulk carbonate at ODP Site 1007 and that of seawater.

Open circles indicate the $\delta^{11}B$ value of bulk carbonate as determined by this study. The analytical error for $\delta^{11}B$ of this study is smaller than the marker size. Filled squares indicate seawater $\delta^{11}B$ values from Pearson and Palmer (2000). The blue curve represents seawater $\delta^{11}B$ values from Greenop et al. (2017), with the darker shadow representing the 68 % confidence interval and the lighter shadow representing the 95 % confidence interval.

most of this B originated from isotopically light seawater borate, porewater $\delta^{11}B$ should in this scenario also decrease. Low-Mg calcite precipitating from ambient porewater would then inherit a lighter $\delta^{11}B$ value than the original aragonite.

This interpretation is also supported by our diagenetic model (fig. 4). In this simulation (fig. 4), boundary condi-

tions such as the initial B/Ca and $\delta^{11}B$ values of carbonates were estimated based on the empirical data reported by Zhang et al. (2017) and this study. Most of the other parameters were obtained from the literature (table 2). A range of values for the rate constant of neomorphism (k_0) and attenuation length for the rate of neomorphism (λ_k) are explored in the model simulations, as they have not been previously constrained. The average sedimentation rate (ω) of the study site is ~0.01 cm yr^{-1}, based on the age model developed from nannofossil and foraminiferal biostratigraphic constraints (Shipboard Scientific Party, 1997). However, the sedimentation rates previously calculated for the upper 300 m range from 0.005 to 0.02 cm yr^{-1} (Shipboard Scientific Party, 1997). As neomorphism occurs chiefly within this same depth range (fig. 2), this variability in sedimentation rate could potentially strongly influence our estimates of neomorphism rate (fig. 5). On the other hand, model runs indicate that changes in λ_k do not strongly influence estimates of neomorphism rate. As shown in figs. 4 and 5, with paired k_0 and ω values, the model can reproduce mineral composition profiles as well as empirical carbonate B/Ca and $\delta^{11}B$ values. Notably, the model results also replicate our empirical observation that the shift in $\delta^{11}B_{carb}$ values extends deeper than that of B/Ca values—bolstering our interpretation that downcore changes in boron geochemistry are driven in large part by neomorphism (fig. 4). Similar decoupling between different components has also been observed for a recently developed 2D model for meteoric diagenesis, likely reflecting a mixing effect between fluid endmembers (M. Y. Zhao, Planavsky, et al., 2020). This suggests that carbonate B/Ca and $\delta^{11}B$ values are nearly in equilibrium with those of ambient porewater. The results displayed in fig. 4 also indicate that the release of boron from carbonates during neomorphism will induce a significant increase in the boron concentration of porewater as well as a decrease in the porewater $\delta^{11}B$ values of total boron, boric acid $B(OH)_3$ and borate ion $B(OH)_4^-$. The $\delta^{11}B_{carb}$ value decreases following neomorphism, due to the preferential uptake of $B(OH)_4^-$ from pore water (fig. 4). The abnormally high B/Ca and $\delta^{11}B_{carb}$ values at 518 mbsf are due to the higher aragonite content of this sample (table 6; Shipboard Scientific Party, 1997).

As shown in fig. 5, the value of k_0 that results in the closest match between model and empirical data increases following an increase in sedimentation rate (ω). For example, the best estimate for the value of k_0 is 2×10^{-6} yr^{-1} when ω = 0.01 cm yr^{-1}, but it increases to ~4×10^{-6} yr^{-1} when ω = 0.02 cm yr^{-1}. Considering the variation in sedimentation rate in the upper 300 m, the best estimate for k_0 should, in this light, be in the range of 1×10^{-6} to 5×10^{-6} yr^{-1}. This compares well with the recrystallization and/or neomorphism rate of shallow water carbonates during subaerial diagenesis, which has been estimated to be in the range of 10^{-6} to 10^{-4} yr^{-1} (James & Choquette, 1984; Matthews, 1968; Steinen & Matthews, 1973; M. Y. Zhao, Planavsky, et al., 2020). These values are higher than the recrystallization rates of deep-sea carbonates, which could be as low as 2×10^{-8} to 4×10^{-9} yr^{-1} (Fantle, 2015; Fantle & DePaolo, 2007). The difference in the reaction rate between carbonate platform and the deep-sea carbonates is likely due to differences in initial carbonate compositions. Modern deep-sea carbonates consist mainly of low-Mg calcite, whereas shallow-water carbonates in platform settings such as the Great Bahama Bank consist largely of high-Mg calcite and aragonite (e.g., Swart & Eberli, 2005). As high-Mg calcite and aragonite are metastable, it is unsurprising that these mineral transformations occur at a higher rate.

Neomorphism occurs well below the sediment-seawater interface (~200 mbsf and deeper) in the study site, suggesting that some triggering factor for the transformation of carbonate minerals must operate at that level, potentially a change in porewater Mg/Ca values (fig. 2; Shipboard Scientific Party, 1997). The decrease in porewater Mg/Ca below 160 m could be driven by the formation of dolomite, which is supported by an increase in the amount of dolomite below this level (fig. 2A). The molar ratio of Mg to Ca has been widely regarded as the most important determining factor for calcium carbonate polymorphism (Balthasar & Cusack, 2015; Hardie, 1996; Stanley & Hardie, 1998). At the seawater temperature measured at Site 1007 (~10 °C; Shipboard Scientific Party, 1997), the laboratory-derived Mg/Ca molar ratio for a dramatic shift from aragonite to calcite is in the range of 3–4 (Balthasar & Cusack, 2015). This compares well with the observed shift of porewater Mg/Ca with depth from 5–6 to <4 across 160 m (fig. 2). These observations further support our interpretation that the change in the distribution of carbonate mineral types across 160 m is driven by the neomorphism of aragonite to calcite rather than a change in the primary (initial) mineral composition of carbonate factory sediments delivered to this site.

Previous work has indicated that there is also lateral fluid flow at Site 1007, as the porewater [Cl^-] concentration increases from a seawater value at 20–30 mbsf to substantially higher values below 100–200 mbsf (Higgins et al., 2018; Shipboard Scientific Party, 1997). This lateral fluid (e.g., a brine) may in turn result in fluid-buffered conditions, responsible for the elevated $\delta^{44}Ca_{carb}$ values observed by previous studies below ~200 mbsf (Higgins et al., 2018). However, since significant B release to pore water is indicated by the down-core decrease we observe in B/Ca values, $\delta^{11}B_{carb}$ values may not be as fluid-buffered as $\delta^{44}Ca_{carb}$ values. Future study of the source, composition and flow rate of this lateral fluid migration, as well as further characterization of the evolution of porewater B signatures with depth will, we hope, help to further constrain the influence of these factors and refine our predictive framework for diagenetic behavior of B/Ca and $\delta^{11}B_{carb}$.

4.3. Implication for the interpretation of ancient $\delta^{11}B_{carb}$ records

Our results have implications for interpreting the B isotopic composition of ancient carbonates. Previous studies have interpreted the $\delta^{11}B$ signatures of ancient bulk carbonates (i.e., the composite signature of all carbonates in a sample) as a reflection of seawater pH and thus atmospheric pCO_2 (e.g., Clarkson et al., 2015; Kasemann et al., 2005, 2010; Ohnemueller et al., 2014). Our results, however, indicate that bulk carbonates can experience a significant $\delta^{11}B$ de-

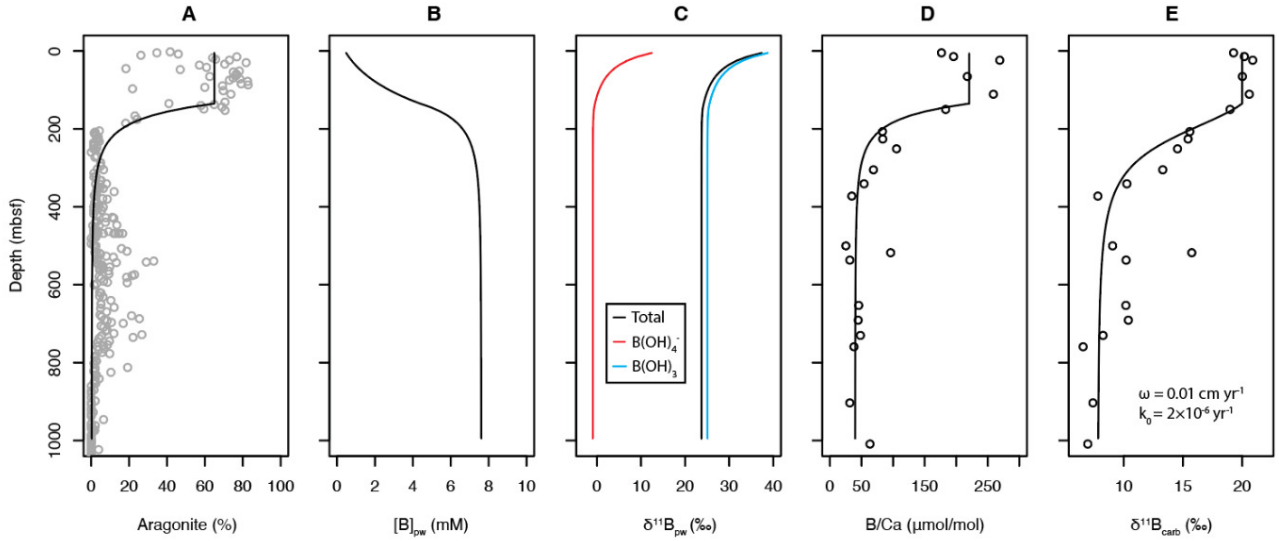

Figure 4. Diagenetic model results and empirical mineralogical and geochemical data for ODP site 1007.

A. Aragonite content. B. [B] of porewater. C. $\delta^{11}B$ values of total B, $B(OH)_4^-$ and $B(OH)_3$ in porewater. D. B/Ca values of bulk carbonate sediments. E. $\delta^{11}B$ of bulk carbonate sediments. Curves represent the results of our diagenetic model; open circles in A, D and E indicate empirical data. Mineralogical data (A) from Shipboard Scientific Party (1997).

Table 6. XRD results of the samples from ODP Site 1007

	Insoluble	Dolomite	Low-Mg calcite	High-Mg calcite	Aragonite	Quartz
	%	%	%	%	%	%
1H	10.7	0	20.2	26.7	41.2	1.3
2H	4.8	0.6	23.7	6.9	64.1	0
3H	5.4	0	18.1	3.6	72.9	0
7H	5.4	0.4	28.2	3.4	62.4	0.3
13X	4.9	0.6	17	3.7	73.3	0.4
17X	4.4	3.4	13.2	8.3	70.7	0
23X	9.4	6.6	81.7	0	1.6	0.6
25X	9.6	8.5	77.4	0	3.7	0.8
28X	8.7	6.5	83	0	1.3	0.5
34X	3.8	1.5	88	0	6.5	0.2
38X	4.3	1.6	91.4	0	2.3	0.4
41X	1.3	0.7	95	0	3	0
21R	4.6	2.2	91.7	0	1.3	0.2
23R	14.6	0.9	64.9	0	18.7	0.9
25R	4	1.4	91.1	0	3.2	0.3
37R	-	-	-	-	-	-
41R	-	-	-	-	-	-
45R	2.8	31.7	60	0	5.4	0
48R	5.2	14.9	76.5	0	3.3	0.1
63R	3.2	0.7	96.1	0	0	0
74R	24.4	4.3	70.4	0	0	0.9

Note: The data are from Shipboard Scientific Party (1997)

crease (as much as 12 ‰—i.e., a change that, in the traditional B isotope framework, might be interpreted as a shift in seawater pH from 8.2 to <7) during marine burial diagenesis. This suggests that even so-called "well-preserved" carbonates that have experienced only marine burial diagenesis may be unable to faithfully preserve seawater-derived $\delta^{11}B_{carb}$ signals. We acknowledge that the degree of alteration in $\delta^{11}B$ is likely to be strongly site-specific

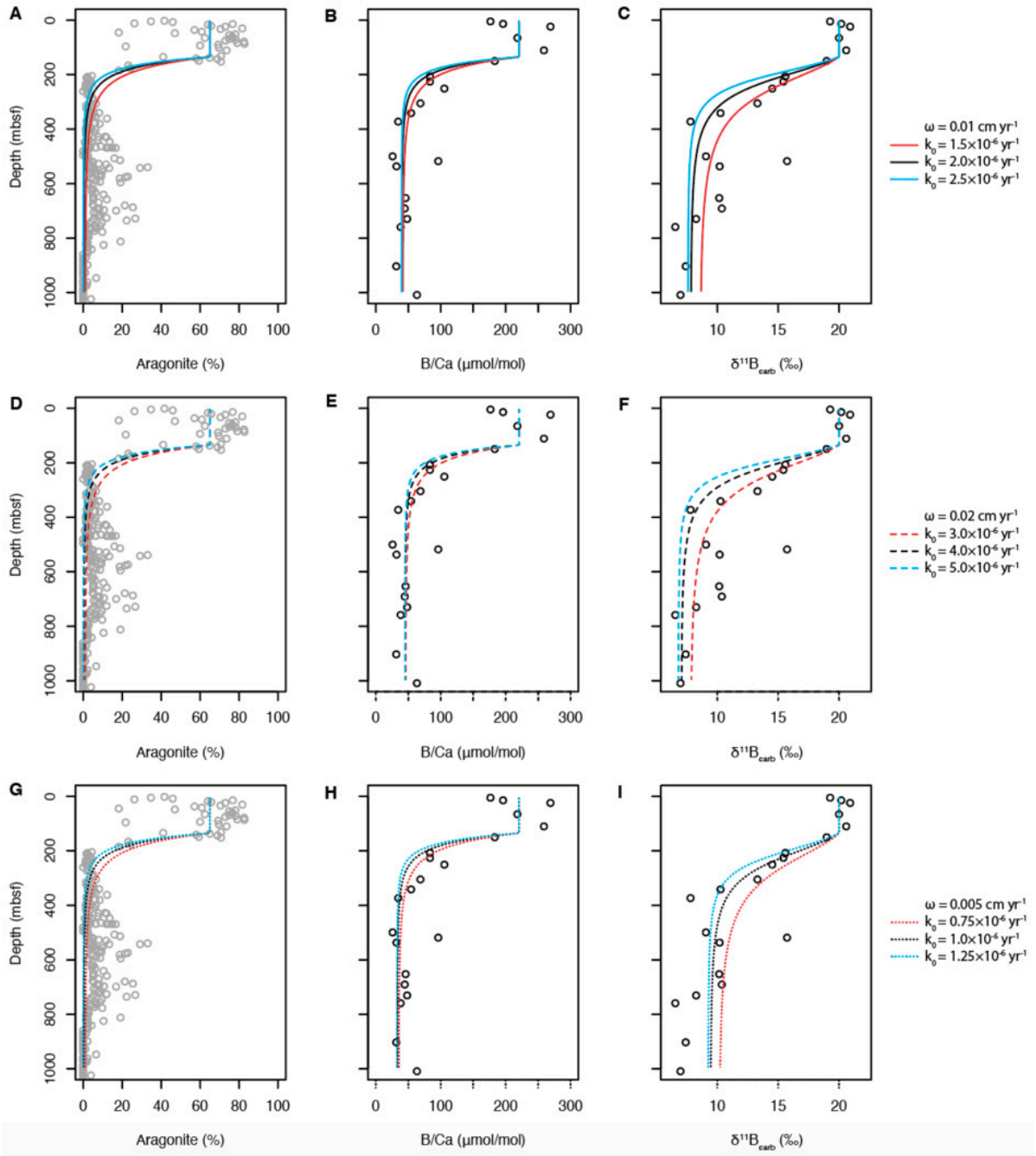

Figure 5. Model results for ODP Site 1007 with varying sedimentation rate and neomorphism rate constant.

A, D, G Aragonite content. B, E, H B/Ca values of bulk carbonate samples. C, F, I $\delta^{11}B$ values of bulk carbonate samples. Curves represent model results, whereas open circles represent empirical data. Mineralogical data from Shipboard Scientific Party (1997).

(Edgar et al., 2015; Spivack et al., 1993; Spivack & You, 1997), depending on the original mineral composition as well as porewater conditions. While recrystallization and decreases in $\delta^{11}B$ values of bulk carbonates have been observed in a deep-sea site dominated by foraminifera and nanofossils (ODP Site 851; Spivack & You, 1997), other studies have not observed similar degrees of B isotopic resetting in other deep-sea sites consisting mainly of foraminiferal calcite (Edgar et al., 2015; Spivack et al., 1993). It is worth noting that the primary low-Mg calcite (~25 % of carbonate sediments in the upper portion of the core; fig. 2) at Site 1007 may not have undergone recrystallization. Thus, *in situ* (and petrographically constrained) measurement of $\delta^{11}B_{carb}$ in primary low-Mg calcites may provide a better record of seawater signals.

Previous studies have found that the B/Ca and $\delta^{11}B$ values of ancient bulk carbonates on continental margins (5 to 30 µmol/mol and -6 to 14 ‰; Clarkson et al., 2015; Kasemann et al., 2005, 2010; Ohnemueller et al., 2014; Vengosh et al., 1991) are much lower than that of modern carbonates deposited in analogous settings (~200 µmol/mol and 20 ‰). This disparity has been variably interpreted to reflect

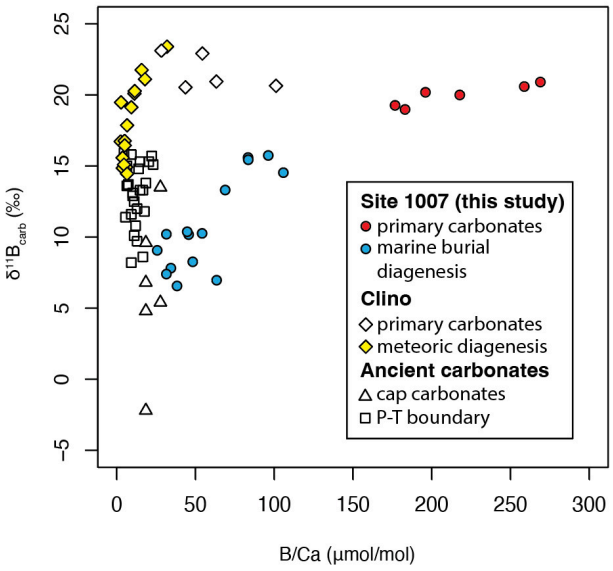

Figure 6. Cross-plot between B/Ca and $\delta^{11}B$ of modern and ancient shallow-water carbonates.

"Primary carbonates" for Site 1007 refer to upper, aragonite-rich portions of the sediment core; "marine burial diagenesis" refers to samples identified by this study as having undergone neomorphism. Data from the Clino core come from Stewart et al. (2015); "primary carbonates" refer to samples which have not experienced significant meteoric diagenesis. Marinoan cap carbonate data from Ohnemueller et al. (2014). Permo-Triassic boundary data from Clarkson et al. (2015).

the influence of terrestrially sourced boron (Vengosh et al., 1991), recrystallization (Ishikawa & Nakamura, 1993) or meteoric diagenesis (Stewart et al., 2015). Our results indicate that, in addition to changes in seawater $\delta^{11}B$ through Earth's history (e.g., Rasbury & Hemming, 2017), neomorphism during marine burial diagenesis could also have contributed to the low B/Ca and $\delta^{11}B$ of ancient bulk carbonates formed on continental margins.

As shown in the cross-plot of B/Ca and $\delta^{11}B$ values of bulk carbonates (fig. 6), carbonates subjected to marine burial diagenesis from ODP Site 1007 show higher B/Ca but even lower $\delta^{11}B$ values than those subjected to meteoric diagenesis in the adjacent but more proximal Clino core (Stewart et al., 2015). This suggests that meteoric diagenesis may not necessarily be associated with lower $\delta^{11}B$ values than marine burial diagenesis, especially when the initial mineral composition is primarily aragonite. Considering the multiple factors shaping both the B/Ca and $\delta^{11}B$ values of carbonates, patterns in B/Ca and $\delta^{11}B$ space (fig. 6) should be considered in the context of independent geochemical evidence—such as mineral composition and carbon and oxygen isotope values—to distinguish between meteoric and marine burial diagenesis. For instance, the $\delta^{18}O_{carb}$ values of the studied ODP Site 1007 are close to 0 ‰ and do not show an obvious negative shift in the whole profile, indicating marine burial diagenesis with limited influence from meteoric water.

4.4. Implication for B isotopes as a proxy for carbonate recrystallization/neomorphism

Our results along with those of Stewart et al. (2015) suggest that recrystallization/neomorphism during both meteoric diagenesis and marine burial diagenesis will have a significant impact on carbonate B isotope signatures. This implies that B isotopes could be a proxy for carbonate recrystallization/neomorphism and original carbonate mineralogy. Since there is a significant drop in B isotopic values during recrystallization/neomorphism from high-Mg calcite and aragonite to low-Mg calcite, B isotopes thus may help to identify recrystallization/neomorphism in ancient carbonates in instances for which ambient seawater $\delta^{11}B$ values can be robustly estimated. The original seawater B isotopic values can be estimated through analysis of known low-Mg calcites (mainly shells).

5. CONCLUSIONS

Geochemical measurements of B/Ca and $\delta^{11}B$ values in modern platform carbonates deposited below the zone of typical meteoric diagenesis (~700 m water depth) indicate that substantial decreases in both B/Ca and $\delta^{11}B$ values can occur during marine burial diagenesis. Multiple lines of evidence, including the B/Ca and $\delta^{11}B$ values of carbonates and porewater Mg/Ca values indicate that notable increases in neomorphism from aragonite to calcite occur at around 200 m below the seafloor. Decreases in $\delta^{11}B$ values with depth are likely due to the release of isotopically light B ($\delta^{11}B$ ~20 ‰) from carbonate to porewater during neomorphism, with subsequent uptake of the isotopically lighter borate ion ($\delta^{11}B$ ~-1 ‰) by the newly formed low-Mg calcite. These interpretations of our empirical data are also supported by numerical diagenetic modeling. Further, our diagenetic model suggests a neomorphism rate in the range of 1×10^{-6} to 5×10^{-6} yr^{-1}, which is similar to the recrystallization and/or neomorphism rates proposed by previous studies for meteoric diagenesis. This significant observed change in $\delta^{11}B$ values during marine burial diagenesis indicates that the $\delta^{11}B$ signature of bulk carbonate sediments does not, in contrast to recent assertions, necessarily provide a simple proxy for the pH of ancient seawater. Our results also imply that B isotopes could be employed as a proxy for carbonate recrystallization/neomorphism and original carbonate mineralogy.

Acknowledgments

We thank Shuang Zhang, Donald Penman and Dan Asael for their assistance with laboratory analyses. M.Z. is funded by the IGGCAS Key programme (no. IGGCAS-202201) and the programme of the Chinese Academy of Sciences (E251520401). NJP acknowledges support from the Packard Foundation. We are grateful to Joe Stewart, Sean Murray and Jesse Farmer for insightful reviews that improved this manuscript.

Data Availability

https://doi.org/10.17632/bxh8gmxp9f.1,
https://data.mendeley.com/datasets/bxh8gmxp9f/1

Editor: C. Page Chamberlain, Associate Editor: Kimberly Lau

Submitted: June 26, 2023 EDT. Accepted: December 02, 2023 EDT. Published: December 31, 2023 EDT.

REFERENCES

Allen, K. A., & Hönisch, B. (2012). The planktic foraminiferal B/Ca proxy for seawater carbonate chemistry: A critical evaluation. *Earth and Planetary Science Letters*, *345–348*, 203–211. https://doi.org/10.1016/j.epsl.2012.06.012

Balthasar, U., & Cusack, M. (2015). Aragonite-calcite seas—Quantifying the gray area. *Geology*, *43*(2), 99–102. https://doi.org/10.1130/g36293.1

Beerling, D. J., & Royer, D. L. (2011). Convergent Cenozoic CO2 history. *Nature Geoscience*, *4*(7), 418–420. https://doi.org/10.1038/ngeo1186

Berner, R. A. (1980). *Early Diagenesis: A Theoretical Approach*. Princeton University Press. https://doi.org/10.1515/9780691209401

Boudreau, B. P. (1997). *Diagenetic Models and their Implementation*. Springer. https://doi.org/10.1007/978-3-642-60421-8

Brown, S. J., & Elderfield, H. (1996). Variations in Mg/Ca and Sr/Ca ratios of planktonic foraminifera caused by postdepositional dissolution: Evidence of shallow Mg-dependent dissolution. *Paleoceanography*, *11*(5), 543–551. https://doi.org/10.1029/96pa01491

Chen, X., Romaniello, S. J., Herrmann, A. D., Hardisty, D., Gill, B. C., & Anbar, A. D. (2018). Diagenetic effects on uranium isotope fractionation in carbonate sediments from the Bahamas. *Geochimica et Cosmochimica Acta*, *237*, 294–311. https://doi.org/10.1016/j.gca.2018.06.026

Clarkson, M. O., Kasemann, S. A., Wood, R. A., Lenton, T. M., Daines, S. J., Richoz, S., Ohnemueller, F., Meixner, A., Poulton, S. W., & Tipper, E. T. (2015). Ocean acidification and the Permo-Triassic mass extinction. *Science*, *348*(6231), 229–232. https://doi.org/10.1126/science.aaa0193

Dellinger, M., Hardisty, D. S., Planavsky, N. J., Gill, B. C., Kalderon-Asael, B., Asael, D., Croissant, T., Swart, P. K., & West, A. J. (2020). The effects of diagenesis on lithium isotope ratios of shallow marine carbonates. *American Journal of Science*, *320*(2), 150–184. https://doi.org/10.2475/02.2020.03

Deyhle, A., & Kopf, A. (2004). Possible influence of clay contamination on B isotope geochemistry of carbonaceous samples. *Applied Geochemistry*, *19*(5), 737–745. https://doi.org/10.1016/j.apgeochem.2003.10.008

Dickson, A. G. (1990). Thermodynamics of the dissociation of boric acid in synthetic seawater from 273.15 to 318.15 K. *Deep Sea Research Part A. Oceanographic Research Papers*, *37*(5), 755–766. https://doi.org/10.1016/0198-0149(90)90004-f

Donald, H. K., Ries, J. B., Stewart, J. A., Fowell, S. E., & Foster, G. L. (2017). Boron isotope sensitivity to seawater pH change in a species of Neogoniolithon coralline red alga. *Geochimica et Cosmochimica Acta*, *217*, 240–253. https://doi.org/10.1016/j.gca.2017.08.021

Edgar, K. M., Anagnostou, E., Pearson, P. N., & Foster, G. L. (2015). Assessing the impact of diagenesis on δ11B, δ13C, δ18O, Sr/Ca and B/Ca values in fossil planktic foraminiferal calcite. *Geochimica et Cosmochimica Acta*, *166*, 189–209. https://doi.org/10.1016/j.gca.2015.06.018

Fantle, M. S. (2015). Calcium isotopic evidence for rapid recrystallization of bulk marine carbonates and implications for geochemical proxies. *Geochimica et Cosmochimica Acta*, *148*, 378–401. https://doi.org/10.1016/j.gca.2014.10.005

Fantle, M. S., & DePaolo, D. J. (2007). Ca isotopes in carbonate sediment and pore fluid from ODP Site 807A: The Ca2+(aq)–calcite equilibrium fractionation factor and calcite recrystallization rates in Pleistocene sediments. *Geochimica et Cosmochimica Acta*, *71*(10), 2524–2546. https://doi.org/10.1016/j.gca.2007.03.006

Fantle, M. S., Maher, K. M., & DePaolo, D. J. (2010). Isotopic Approaches for Quantifying the Rates of Marine Burial Diagenesis. *Reviews of Geophysics*, *48*(3). https://doi.org/10.1029/2009rg000306

Foster, G. L. (2008). Seawater pH, pCO2 and [CO2−3] variations in the Caribbean Sea over the last 130 kyr: A boron isotope and B/Ca study of planktic foraminifera. *Earth and Planetary Science Letters*, *271*(1–4), 254–266. https://doi.org/10.1016/j.epsl.2008.04.015

Frank, T. D., & Bernet, K. (2000). Isotopic signature of burial diagenesis and primary lithological contrasts in periplatform carbonates (Miocene, Great Bahama Bank). *Sedimentology*, *47*(6), 1119–1134. https://doi.org/10.1046/j.1365-3091.2000.00344.x

Greenop, R., Hain, M. P., Sosdian, S. M., Oliver, K. I. C., Goodwin, P., Chalk, T. B., Lear, C. H., Wilson, P. A., & Foster, G. L. (2017). A record of Neogene seawater δ11B reconstructed from paired δ11B analyses on benthic and planktic foraminifera. *Climate of the Past*, *13*(2), 149–170. https://doi.org/10.5194/cp-13-149-2017

Gutjahr, M., Bordier, L., Douville, E., Farmer, J., Foster, G. L., Hathorne, E. C., Hönisch, B., Lemarchand, D., Louvat, P., McCulloch, M., Noireaux, J., Pallavicini, N., Rae, J. W. B., Rodushkin, I., Roux, P., Stewart, J. A., Thil, F., & You, C.-F. (2021). Sub-Permil Interlaboratory Consistency for Solution-Based Boron Isotope Analyses on Marine Carbonates. *Geostandards and Geoanalytical Research*, *45*(1), 59–75. https://doi.org/10.1111/ggr.12364

Hardie, L. A. (1996). Secular variation in seawater chemistry: An explanation for the coupled secular variation in the mineralogies of marine limestones and potash evaporites over the past 600 m.y. *Geology*, *24*(3), 279–283.

Hemming, N. G., & Hanson, G. N. (1992). Boron Isotopic Composition and Concentration in Modern Marine Carbonates. *Geochimica et Cosmochimica Acta*, *56*(1), 537–543. https://doi.org/10.1016/0016-7037(92)90151-8

Henehan, M. J., Foster, G. L., Bostock, H. C., Greenop, R., Marshall, B. J., & Wilson, P. A. (2016). A new boron isotope-pH calibration for Orbulina universa, with implications for understanding and accounting for 'vital effects.' *Earth and Planetary Science Letters*, *454*, 282–292. https://doi.org/10.1016/j.epsl.2016.09.024

Henehan, M. J., Klein Gebbinck, C. D., Wyman, J. V. B., Hain, M. P., Rae, J. W. B., Hönisch, B., Foster, G. L., & Kim, S.-T. (2022). No ion is an island: Multiple ions influence boron incorporation into CaCO3. *Geochimica et Cosmochimica Acta*, *318*, 510–530. https://doi.org/10.1016/j.gca.2021.12.011

Henehan, M. J., Ridgwell, A., Thomas, E., Zhang, S., Alegret, L., Schmidt, D. N., Rae, J. W. B., Witts, J. D., Landman, N. H., Greene, S. E., Huber, B. T., Super, J. R., Planavsky, N. J., & Hull, P. M. (2019). Rapid ocean acidification and protracted Earth system recovery followed the end-Cretaceous Chicxulub impact. *Proceedings of the National Academy of Sciences of the United States of America*, *116*(45), 22500–22504. https://doi.org/10.1073/pnas.1905989116

Higgins, J. A., Blättler, C. L., Lundstrom, E. A., Santiago-Ramos, D. P., Akhtar, A. A., Crüger Ahm, A.-S., Bialik, O., Holmden, C., Bradbury, H., Murray, S. T., & Swart, P. K. (2018). Mineralogy, early marine diagenesis, and the chemistry of shallow-water carbonate sediments. *Geochimica et Cosmochimica Acta*, *220*, 512–534. https://doi.org/10.1016/j.gca.2017.09.046

Ishikawa, T., & Nakamura, E. (1993). Boron isotope systematics of marine sediments. *Earth and Planetary Science Letters*, *117*(3–4), 567–580. https://doi.org/10.1016/0012-821x(93)90103-g

James, N. P., & Choquette, P. W. (1984). Diagenesis .9. Limestones - the Meteoric Diagenetic Environment. *Geoscience Canada*, *11*(4), 161–194. https://id.erudit.org/iderudit/geocan11_4art01

Kasemann, S. A., Hawkesworth, C. J., Prave, A. R., Fallick, A. E., & Pearson, P. N. (2005). Boron and calcium isotope composition in Neoproterozoic carbonate rocks from Namibia: evidence for extreme environmental change. *Earth and Planetary Science Letters*, *231*(1–2), 73–86. https://doi.org/10.1016/j.epsl.2004.12.006

Kasemann, S. A., Prave, A. R., Fallick, A. E., Hawkesworth, C. J., & Hoffmann, K.-H. (2010). Neoproterozoic ice ages, boron isotopes, and ocean acidification: Implications for a snowball Earth. *Geology*, *38*(9), 775–778. https://doi.org/10.1130/g30851.1

Klochko, K., Cody, G. D., Tossell, J. A., Dera, P., & Kaufman, A. J. (2009). Re-evaluating boron speciation in biogenic calcite and aragonite using 11B MAS NMR. *Geochimica et Cosmochimica Acta*, *73*(7), 1890–1900. https://doi.org/10.1016/j.gca.2009.01.002

Klochko, K., Kaufman, A. J., Yao, W., Byrne, R. H., & Tossell, J. A. (2006). Experimental measurement of boron isotope fractionation in seawater. *Earth and Planetary Science Letters*, *248*(1–2), 276–285. https://doi.org/10.1016/j.epsl.2006.05.034

Knauth, L. P., & Kennedy, M. J. (2009). The late Precambrian greening of the Earth. *Nature*, *460*(7256), 728–732. https://doi.org/10.1038/nature08213

Land, L. S. (1986). Limestone diagenesis — some geochemical considerations. *U.S. Geological Survey Bulletin*, *1578*, 129–137. https://doi.org/10.3133/b1578

Liu, X.-M., Hardisty, D. S., Lyons, T. W., & Swart, P. K. (2019). Evaluating the fidelity of the cerium paleoredox tracer during variable carbonate diagenesis on the Great Bahamas Bank. *Geochimica et Cosmochimica Acta*, *248*, 25–42. https://doi.org/10.1016/j.gca.2018.12.028

Malone, M. J., Slowey, N. C., & Henderson, G. M. (2001). Early diagenesis of shallow-water periplatform carbonate sediments, leeward margin, Great Bahama Bank (Ocean Drilling Program Leg 166). *Geological Society of America Bulletin*, *113*(7), 881–894.

Marshall, J. D. (1992). Climatic and oceanographic isotopic signals from the carbonate rock record and their preservation. *Geological Magazine*, *129*(2), 143–160. https://doi.org/10.1017/s0016756800008244

Matthews, R. K. (1968). Carbonate diagenesis: Equilibration of sedimentary mineralogy to the subaerial environment; coral cap of Barbados, West Indies. *Journal of Sedimentary Research*, *38*(4), 1110–1119. https://doi.org/10.1306/74d71b13-2b21-11d7-8648000102c1865d

McCulloch, M. T., Holcomb, M., Rankenburg, K., & Trotter, J. A. (2014). Rapid, high-precision measurements of boron isotopic compositions in marine carbonates. *Rapid Communications in Mass Spectrometry*, *28*(24), 2704–2712. https://doi.org/10.1002/rcm.7065

Melim, L. A., Westphal, H., Swart, P. K., Eberli, G. P., & Munnecke, A. (2002). Questioning carbonate diagenetic paradigms: evidence from the Neogene of the Bahamas. *Marine Geology*, *185*(1–2), 27–53. https://doi.org/10.1016/s0025-3227(01)00289-4

Nir, O., Vengosh, A., Harkness, J. S., Dwyer, G. S., & Lahav, O. (2015). Direct measurement of the boron isotope fractionation factor: Reducing the uncertainty in reconstructing ocean paleo-pH. *Earth and Planetary Science Letters*, *414*, 1–5. https://doi.org/10.1016/j.epsl.2015.01.006

Noireaux, J., Mavromatis, V., Gaillardet, J., Schott, J., Montouillout, V., Louvat, P., Rollion-Bard, C., & Neuville, D. R. (2015). Crystallographic control on the boron isotope paleo-pH proxy. *Earth and Planetary Science Letters*, *430*, 398–407. https://doi.org/10.1016/j.epsl.2015.07.063

Oehlert, A. M., & Swart, P. K. (2014). Interpreting carbonate and organic carbon isotope covariance in the sedimentary record. *Nature Communications*, *5*(1). https://doi.org/10.1038/ncomms5672

Ohnemueller, F., Prave, A. R., Fallick, A. E., & Kasemann, S. A. (2014). Ocean acidification in the aftermath of the Marinoan glaciation. *Geology*, *42*(12), 1103–1106. https://doi.org/10.1130/g35937.1

Paris, G., Bartolini, A., Donnadieu, Y., Beaumont, V., & Gaillardet, J. (2010). Investigating boron isotopes in a middle Jurassic micritic sequence: Primary vs. diagenetic signal. *Chemical Geology*, *275*(3–4), 117–126. https://doi.org/10.1016/j.chemgeo.2010.03.013

Pearson, P. N., & Palmer, M. R. (2000). Atmospheric carbon dioxide concentrations over the past 60 million years. *Nature*, *406*(6797), 695–699. https://doi.org/10.1038/35021000

Rae, J. W. B., Foster, G. L., Schmidt, D. N., & Elliott, T. (2011). Boron isotopes and B/Ca in benthic foraminifera: Proxies for the deep ocean carbonate system. *Earth and Planetary Science Letters*, *302*(3–4), 403–413. https://doi.org/10.1016/j.epsl.2010.12.034

Rae, J. W. B., Zhang, Y. G., Liu, X. Q., Foster, G. L., Stoll, H. M., & Whiteford, R. D. M. (2021). Atmospheric CO_2 over the Past 66 Million Years from Marine Archives. *Annual Review of Earth and Planetary Sciences*, *49*(1), 609–641. https://doi.org/10.1146/annurev-earth-082420-063026

Rasbury, E. T., & Hemming, N. G. (2017). Boron Isotopes: A "Paleo-pH Meter" for Tracking Ancient Atmospheric CO2. *Elements*, *13*(4), 243–248. https://doi.org/10.2138/gselements.13.4.243

Schlitzer, R. (2018). *Ocean Data View*. https://odv.awi.de

Sen, S., Stebbins, J. F., Hemming, N. G., & Ghosh, B. (1994). Coordination Environments of B-Impurities in Calcite and Aragonite Polymorphs - a B-11 Mas Nmr-Study. *American Mineralogist*, *79*(9–10), 819–825.

Shipboard Scientific Party. (1997). Site 1007. In G. P. Eberli, P. K. Swart, & M. J. Malone (Eds.), *Proceedings of the Ocean Drilling Program, 166 Initial Reports* (pp. 289–345). Ocean Drilling Program. https://doi.org/10.2973/odp.proc.ir.166.110.1997

Soetaert, K., Petzoldt, T., & Setzer, R. W. (2010). Solving differential equations in R: Package deSolve. *Journal of Statistical Software*, *33*(9), 1–25. https://doi.org/10.18637/jss.v033.i09

Spivack, A. J., & You, C.-F. (1997). Boron isotopic geochemistry of carbonates and pore waters, Ocean Drilling Program Site 851. *Earth and Planetary Science Letters*, *152*(1–4), 113–122. https://doi.org/10.1016/s0012-821x(97)00134-9

Spivack, A. J., You, C.-F., & Smith, H. J. (1993). Foraminiferal boron isotope ratios as a proxy for surface ocean pH over the past 21 Myr. *Nature*, *363*(6425), 149–151. https://doi.org/10.1038/363149a0

Stanley, S. M., & Hardie, L. A. (1998). Secular oscillations in the carbonate mineralogy of reef-building and sediment-producing organisms driven by tectonically forced shifts in seawater chemistry. *Palaeogeography, Palaeoclimatology, Palaeoecology*, *144*(1–2), 3–19. https://doi.org/10.1016/s0031-0182(98)00109-6

Steinen, R. P., & Matthews, R. K. (1973). Phreatic Vs Vadose Diagenesis - Stratigraphy and Mineralogy of a Cored Borehole on Barbados, Wi. *Journal of Sedimentary Petrology*, *43*(4), 1012–1020.

Stewart, J. A., Christopher, S. J., Kucklick, J. R., Bordier, L., Chalk, T. B., Dapoigny, A., Douville, E., Foster, G. L., Gray, W. R., Greenop, R., Gutjahr, M., Hemsing, F., Henehan, M. J., Holdship, P., Hsieh, Y.-T., Kolevica, A., Lin, Y.-P., Mawbey, E. M., Rae, J. W. B., … Day, R. D. (2021). NIST RM 8301 Boron Isotopes in Marine Carbonate (Simulated Coral and Foraminifera Solutions): Inter-laboratory $\delta^{11}B$ and Trace Element Ratio Value Assignment. *Geostandards and Geoanalytical Research*, *45*(1), 77–96. https://doi.org/10.1111/ggr.12363

Stewart, J. A., Gutjahr, M., Pearce, F., Swart, P. K., & Foster, G. L. (2015). Boron during meteoric diagenesis and its potential implications for Marinoan snowball Earth δ11B-pH excursions. *Geology*, *43*(7), 627–630. https://doi.org/10.1130/g36652.1

Swart, P. K. (2008). Global synchronous changes in the carbon isotopic composition of carbonate sediments unrelated to changes in the global carbon cycle. *Proceedings of the National Academy of Sciences of the United States of America*, *105*(37), 13741–13745. https://doi.org/10.1073/pnas.0802841105

Swart, P. K., & Eberli, G. (2005). The nature of the δ13C of periplatform sediments: Implications for stratigraphy and the global carbon cycle. *Sedimentary Geology*, *175*(1–4), 115–129. https://doi.org/10.1016/j.sedgeo.2004.12.029

Tarhan, L. G., Zhao, M., & Planavsky, N. J. (2021). Bioturbation feedbacks on the phosphorus cycle. *Earth and Planetary Science Letters*, *566*, 116961. https://doi.org/10.1016/j.epsl.2021.116961

Vengosh, A., Kolodny, Y., Starinsky, A., Chivas, A. R., & McCulloch, M. T. (1991). Coprecipitation and Isotopic Fractionation of Boron in Modern Biogenic Carbonates. *Geochimica et Cosmochimica Acta*, *55*(10), 2901–2910. https://doi.org/10.1016/0016-7037(91)90455-e

Vogl, J., & Rosner, M. (2012). Production and Certification of a Unique Set of Isotope and Delta Reference Materials for Boron Isotope Determination in Geochemical, Environmental and Industrial Materials. *Geostandards and Geoanalytical Research*, *36*(2), 161–175. https://doi.org/10.1111/j.1751-908x.2011.00136.x

Zhang, S., Henehan, M. J., Hull, P. M., Reid, R. P., Hardisty, D. S., Hood, A. v.S., & Planavsky, N. J. (2017). Investigating controls on boron isotope ratios in shallow marine carbonates. *Earth and Planetary Science Letters*, *458*, 380–393. https://doi.org/10.1016/j.epsl.2016.10.059

Zhao, M., Tarhan, L., Planavsky, N., & Isson, T. (2023). The influence of warming on phosphorus burial in continental margin sediments. *American Journal of Science*, *323*, 6. https://doi.org/10.2475/001c.85110

Zhao, M. Y., Blake, R. E., Liang, Y. H., Ruf, D. D., Jaisi, D. P., Chang, S. J., & Planavsky, N. J. (2021). Oxygen isotopic fingerprints on the phosphorus cycle within the deep subseafloor biosphere. *Geochimica et Cosmochimica Acta*, *310*, 169–186. https://doi.org/10.1016/j.gca.2021.05.018

Zhao, M. Y., Planavsky, N., Oehlert, A. M., Wei, G. Y., & Gong, Z. (2020). Simulating Meteoric and Mixing Zone Carbonate Diagenesis with a Two-Dimensional Reactive Transport Model. *American Journal of Science*, *320*(7), 599–636. https://doi.org/10.2475/09.2020.02

Zhao, M. Y., Zhang, S., Tarhan, L. G., Reinhard, C. T., & Planavsky, N. (2020). The role of calcium in regulating marine phosphorus burial and atmospheric oxygenation. *Nature Communications*, *11*(1), 2232. https://doi.org/10.1038/s41467-020-15673-3

Zhao, M. Y., & Zheng, Y. F. (2014). Marine carbonate records of terrigenous input into Paleotethyan seawater: Geochemical constraints from Carboniferous limestones. *Geochimica et Cosmochimica Acta*, *141*, 508–531. https://doi.org/10.1016/j.gca.2014.07.001

Zhao, M. Y., & Zheng, Y. F. (2017). A geochemical framework for retrieving the linked depositional and diagenetic histories of marine carbonates. *Earth and Planetary Science Letters*, *460*, 213–221. https://doi.org/10.1016/j.epsl.2016.11.033

SUPPLEMENTARY MATERIALS

Resetting of shallow-water carbonate boron isotope values during marine burial diagenesis

Download: https://ajsonline.org/article/91398-resetting-of-shallow-water-carbonate-boron-isotope-values-during-marine-burial-diagenesis/attachment/223513.docx